# Robust SAV-Ensemble algorithms for parametrized flow problems with energy stable open boundary conditions

Nan Jiang <sup>a,1</sup>, Aziz Takhirov<sup>b,2,\*</sup>, Jiajia Waters<sup>c</sup>

<sup>a</sup>Department of Mathematics, University of Florida, Gainesville, FL 32611, USA
 <sup>b</sup>Department of Mathematics, University of Sharjah, UAE
 <sup>c</sup>Los Alamos National Laboratory, Los Alamos, NM 87545, USA

#### Abstract

In this report we propose fast and robust ensemble simulation algorithms for parametrized nonlinear flow problems with open boundaries. We synthesize the recent SAV idea, the ensemble timestepping and the energy stable open boundary conditions, and develop efficient ensemble algorithms that only require a single matrix assembly for all realizations and all time steps. Moreover, the proposed algorithms are unconditionally stable without any restricting assumptions on the variance of the viscosities or the time steps, and they always produce positive values for the auxiliary variables. The second order algorithm is numerically tested on three benchmark flow problems with open boundaries, and is shown to be both accurate and effective in preventing the backflow instabilities.

Keywords: Ensemble simulations, open boundary conditions, incompressible Navier-Stokes Equations, Scalar Auxilar Variable

2010 MSC: 65M60, 76D05

<sup>\*</sup>Corresponding author

 $Email\ addresses: \verb|jiangnQufl.edu| (Nan\ Jiang\ ), \verb|atakhirovQsharjah.ac.ae| (Aziz\ Takhirov), \verb|jwatersQlanl.gov| (Jiajia\ Waters)$ 

 $<sup>^1{\</sup>rm This}$  author was partially supported by the US National Science Foundation grants DMS-1720001 and DMS-2120413

 $<sup>^2\</sup>mathrm{This}$  author was partially supported by the University of Sharjah Seed Research Project no. 21021440101

#### 1. Introduction

With improved algorithms and faster computer power, the focus is shifting from simply analyzing a model for one set of input data, to characterizing its behavior at "nearby" sets of data. Moreover, the engineers must have an idea of how the flow responds to changes in the parameters or assess the effect of input data uncertainty on the response of the system. Such and other scenarios lead to the problem of solving an ensemble of flow equations. Some specific examples are sensitivity studies [1], turbulence modeling for non-homogeneous flows [2], combustion [3], numerical weather prediction [4, 5].

In this work, we consider solving an ensemble of incompressible Navier-Stokes equations subject to perturbed initial conditions  $u_j^0$ , body forces  $f_j$  and viscosity coefficients  $\nu_j$ ,  $j = \overline{1, J}$ :

$$\partial_t u_j + u_j \cdot \nabla u_j - \nabla \cdot (\nu_j(x) \nabla u_j) + \nabla p_j = f_j(x, t) \text{ in } \Omega, \tag{1}$$

$$\nabla \cdot u_i = 0 \text{ in } \Omega, \tag{2}$$

$$u_i = g_i(x, t) \text{ on } \Gamma_D,$$
 (3)

$$(-\nu_j \nabla u_j + p_j \mathbf{I}) \mathbf{n} = \mathbf{S}_{\Gamma} (u_j, p_j) \text{ on } \Gamma_N,$$
 (4)

$$u_i(x,0) = u_i^0(x) \text{ in } \Omega, \tag{5}$$

where  $\Omega$  denotes the flow domain, and  $\Gamma$  is its boundary. We assume that  $\Gamma$  is decomposed into non-overlapping Dirichlet  $\Gamma_D$  and Neumann (open)  $\Gamma_N$  boundaries. The choice of the stabilization term  $S_{\Gamma}(u_j, p_j)$  will be discussed in the next section.

When solving (1)-(5), one can achieve unconditional stability with fully implicit or implicit-explicit schemes [6]. However, this would require assembly and storage of J coefficient matrices at each time step. On the other hand, in the case of  $\nu_j = \nu$ , one can treat the nonlinear term fully explicitly, and thereby assemble a single coefficient matrix once for all. The resulting linear systems could be solved efficiently using solvers for systems with multiple right-hand sides, cf. [7, 8]. But this often induces a very restrictive timestep condition, especially on adaptively refined meshes.

One alternative to the fully explicit approach was proposed in [9], which considered the  $\nu_j = \nu = \text{const}$  case. The scheme was first order in time, and suitable for low Re number flows. The idea was later extended to higher order schemes and high Re flows in [10, 11, 12]. The common idea in all of these references is to split the nonlinear term into semi-implicit and fully explicit parts, where the former is advected by lagged ensemble mean and the latter is advected by lagged fluctuating velocity. The energy stability then can be shown to hold under a timestep restriction involving the velocity fluctuations, which should not be as restrictive as the fully explicit approach. The case of the multiple viscosity coefficients has been addressed in [13, 14, 15], which place an additional condition on the magnitude of the viscosity variance.

Since the introduction of the Scalar Auxiliary Variable (SAV) method for gradient flows in [16], the development of unconditionally stable schemes with explicitly treated nonlinear term has received a lot of interest in the literature. Starting from the initial work of [17], a different variation of SAV-based schemes for solving incompressible Navier-Stokes system have been proposed in [18, 19, 20]. The underlying idea of the SAV-based schemes is to introduce an additional ordinary differential equation (ODE) to the governing system for the SAV, lag the whole nonlinear term and cancel it out in the stability analysis by having the same nonlinear term in the discrete scheme for the ODE of the SAV. However, even though all the existing schemes are unconditionally stable, to our best knowledge and experience, none of them could be viewed as robust. While some schemes are not even guaranteed to produce positive or real-valued approximations of scalar auxiliary variables, others have been observed to produce non-convergent solutions. Note that if there was a robust SAV scheme, then efficiently solving the system (1)-(5) for the  $\nu_i = \nu$  case would be immediate, as there will be a single matrix to assemble and to store with J right hand sides. Such systems can efficiently be solved using block iterative solvers.

One remedy to address these deficiencies of the SAV schemes was put forth in a recent paper [21], for ensembles when  $\Gamma_N = \emptyset$ . The addition of classical Voigt regularization term [22, 23] was observed to improve the accuracy of the

SAV methods, but the ODE for the auxiliary variable was not always solvable. In this report, we synthesize the ideas developed in [18, 21, 14], and develop SAV-ensemble calculation schemes that require only a *single* matrix assembly for all realizations and all time steps, are unconditionally stable without any restricting assumptions on the variance of viscosities  $\nu_j$  or the time steps, and always produce positive values for the auxiliary variables.

This paper is organized as follows. In Section 2, we introduce the notations and discuss the open boundary conditions. In Section 3, we derive the numerical schemes and discuss their stabilities. In Section 4, we present the solution method of our schemes. We will then test our schemes in Section 5 and wrap up the manuscript with conclusions in Section 6.

#### 2. Preliminaries

#### 55 2.1. Notations

Given an ensemble of realizations  $g_1(x), ..., g_J(x)$  of a quantity g(x), we define the fluctuation in j-th member as

$$g_{j}'(x) = g_{j}(x) - \overline{g}(x),$$

and its maximum value by

$$g_{\infty} = \max_{1 \le j \le J} \sup_{x \in \Omega} g_j(x).$$

The normal component of stress tensor and its modification will be denoted by

$$\sigma(u_j, p_j) := -\nu_j \nabla u_j \cdot \mathbf{n} + p_j \mathbf{n}, \qquad \widehat{\sigma}(u_j, p_j) = \sigma(u_j, p_j) - \frac{u_j \cdot \mathbf{n}}{2} u_j.$$

The  $L^2(\Omega)$  norm and inner product will be denoted by  $\|\cdot\|$  and  $(\cdot, \cdot)$ , while the  $L^2$  inner product over  $\Gamma_D$  and  $\Gamma_N$  will be denoted by  $(\cdot, \cdot)_D$  and  $(\cdot, \cdot)_N$ , respectively. For simplicity of the presentation, we assume no-slip boundary condition on  $\Gamma_D$  in the stability analysis. In this setting, the appropriate velocity and pressure spaces are defined as

$$X := \left\{ v \in \left(H^1(\Omega)\right)^d : v = 0 \text{ on } \Gamma_D \right\}, \ Q := L^2(\Omega).$$

We use as the norm on X, the seminorm  $\|\nabla \cdot\|_{L^2}$ .

The dual space  $X^* = H_D^{-1}(\Omega)$  is equipped with norm

$$||f||_{-1,*} = \sup_{v \in X} \frac{\langle f, v \rangle}{||\nabla v||},$$

where  $\langle \cdot, \cdot \rangle$  refers to a duality pairing.

To simplify the notations, we assume that the approximation is continuous in space.

Explicitly skew-symmetrized nonlinear term will be denoted by

$$b_1(u, v, w) := (u \cdot \nabla v, w) + \frac{1}{2}(\nabla \cdot u, w \cdot v).$$

Integration by parts formula shows that

$$b_1(u, v, w) = (u \cdot \mathbf{n}, v \cdot w)_{\Gamma} - b_1(u, w, v), \tag{6}$$

which in particular implies that

$$b_1(u, v, v) = \left(\frac{u \cdot \mathbf{n}}{2}, |v|^2\right)_{\Gamma}.$$
 (7)

# 2.2. Open boundary conditions

Open boundary conditions (4) are often used to truncate a big physical domain to make the problem tractable, or when the flow domain is unbounded, such as in jet flows. The review of the topic for incompressible flows can be found in [24, 25, 26]. Our choice of  $S_{\Gamma}$  used in this work was proposed and benchmarked in [27, 28]. It belongs to a family of velocity-penalization boundary conditions, and has been also successfully tested in physiological regimes as well [26].

To discuss our choice of open boundary condition, for  $0 < \varepsilon \ll 1$  we introduce a smoothed Heaviside function and its opposite:

$$\Theta_{1}(x) := \frac{1}{2} \left( 1 + \tanh \frac{x}{\varepsilon} \right) \simeq H(x), 
\Theta_{0}(x) := \frac{1}{2} \left( 1 - \tanh \frac{x}{\varepsilon} \right) \simeq 1 - H(x).$$
(8)

In this paper, we will consider schemes based on the following open boundary condition:

$$S_{\Gamma}(u_j, p_j) := -\frac{\Theta_0(u_j \cdot \mathbf{n}) u_j \cdot \mathbf{n}}{2} u_j \text{ on } \Gamma_N,$$
(9)

where it is assumed that the velocity  $u_j$  is properly non-dimensionalized. Otherwise,  $\Theta_0\left(\frac{u_j \cdot \mathbf{n}}{U_0}\right)$  must be used in (9), for some reference speed  $U_0$ .

To understand the boundary condition (9), let us partitition  $\Gamma_N$  into outflow and backflow regions:

$$\Gamma_N = \Gamma_{i,N}^+ \cap \Gamma_{i,N}^-$$
, where

$$\Gamma_{j,N}^{+}:=\left\{x\in\Gamma_{N}:\left(u_{j}\cdot\mathbf{n}\right)\left(x\right)>0\right\}\ \text{and}\ \Gamma_{j,N}^{-}:=\left\{x\in\Gamma_{N}:\left(u_{j}\cdot\mathbf{n}\right)\left(x\right)\leq0\right\}.$$

Then (9) is equivalent to

$$(-\nu_j \nabla u_j + p_j \mathbf{I}) \mathbf{n} \simeq \begin{cases} 0, & \text{if } x \in \Gamma_{j,N}^+, \\ -\frac{u_j \cdot \mathbf{n}}{2} u_j, & \text{if } x \in \Gamma_{j,N}^-, \end{cases}$$

hence an alternative name, directional do-nothing condition [29].

The open boundary condition in the weak formulation will be implemented via the following trilinear term:

$$b_2(u,v,w) := -\frac{1}{2}((u \cdot \mathbf{n})\Theta_0(u \cdot \mathbf{n}), v \cdot w)_N.$$

# 3. Numerical schemes

## 3.1. First order scheme

Define the scalar auxiliary variables by

$$E_j = \frac{\|u_j\|^2}{2} + C_0, \qquad R_j^2 = E_j, \quad \xi_j = \frac{R_j^2}{E_j} = 1, \qquad j = 1, \dots, J.$$
 (10)

Motivated by an earlier paper [14] on ensemble calculations, we consider the following perturbation of the momentum equation (1) and the open boundary condition (9):

$$\partial_t u_j + \xi_j u_j \cdot \nabla u_j - \nu_j \Delta u_j - \tau \widehat{\nu} \Delta \partial_t u_j + \nabla p_j = f_j \tag{11}$$

and

$$\underbrace{\left(-\nu_{j}\nabla u_{j} - \widehat{\nu}\tau\nabla\partial_{t}u_{j} + p_{j}\mathbf{I}\right)\mathbf{n}}_{:=\sigma_{1}\left(u_{j},p_{j}\right)} = -\xi_{j}\frac{\Theta_{0}\left(u_{j}\cdot\mathbf{n}\right)u_{j}\cdot\mathbf{n}}{2}u_{j} \text{ on } \Gamma_{N},$$
(12)

where  $\widehat{\nu} := \nu_{\infty} + \alpha, \alpha > 0$ .

Upon multiplying (11) by a test function  $v \in H^1(\Omega)$  and integrating by parts, we obtain

$$(\partial_t u_j, v) + \xi_j \sum_{i=1}^2 b_i(u_j, u_j, v) + \nu_j (\nabla u_j, \nabla v) + \tau \widehat{\nu} (\nabla \partial_t u_j, \nabla v) - (p_j, \nabla \cdot v) + \langle \sigma_1(u_j, p_j), v \rangle_D = \langle f_j, v \rangle.$$

$$(13)$$

Thus the equation for  $R_j$  can be written as

$$2R_{j}\partial_{t}R_{j} = (\partial_{t}u_{j}, u_{j})$$

$$= (\partial_{t}u_{j}, u_{j}) + \xi_{j} \sum_{i=1}^{2} b_{i} (u_{j}, u_{j}, u_{j}) - \left\langle \frac{g_{j} \cdot \mathbf{n}}{2} g_{j}, g_{j} \right\rangle_{D}$$

$$- \xi_{j} \left\langle \frac{\Theta_{1} (u_{j} \cdot \mathbf{n}) u_{j} \cdot \mathbf{n}}{2}, |u_{j}|^{2} \right\rangle_{N} \text{ (now use (13) with } v = u_{j})$$

$$= -\xi_{j} \nu_{j} ||\nabla u_{j}||^{2} - \tau \xi_{j} \widehat{\nu} \partial_{t} \frac{||\nabla u_{j}||^{2}}{2} - \xi_{j} \left\langle \frac{\Theta_{1} (u_{j} \cdot \mathbf{n}) u_{j} \cdot \mathbf{n}}{2}, |u_{j}|^{2} \right\rangle_{N}$$

$$- \left\langle \widehat{\sigma}_{1} (u_{j}, p_{j}), g_{j} \right\rangle_{D} + (f_{j}, u_{j}),$$

where  $\hat{\sigma}_1(u_j, p_j) := \sigma_1(u_j, p_j) + \frac{g_j \cdot \mathbf{n}}{2} g_j$ . Note that when  $f_j = g_j = 0$ , integrating (14) over time from 0 to t, we get the unconditional stability of the SAV ensemble scheme (13)-(14):

$$\left(R_j^2(t) + \tau \xi_j \widehat{\nu} \frac{\|\nabla u_j\|^2}{2}\right) - \left(R_j^2(0) + \tau \xi_j \widehat{\nu} \frac{\|\nabla u_j^0\|^2}{2}\right)$$

$$= -\xi_j \int_0^t \left[\nu_j \|\nabla u_j\|^2 + \left\langle \frac{\Theta_1\left(u_j \cdot \mathbf{n}\right) u_j \cdot \mathbf{n}}{2}, |u_j|^2 \right\rangle_N\right] ds.$$
(15)

Now we will use the equations (13)-(14) to derive the first-order scheme. Discretizing the equation (13) with the test functions from  $X_D$  gives

$$\left(\frac{u_j^{n+1} - u_j^n}{\tau}, v\right) + \xi_j^{n+1} \sum_{i=1}^2 b_i(u_j^n, u_j^n, v) + \nu_j \left(\nabla u_j^n, \nabla v\right) - \left(p_j^{n+1}, \nabla \cdot v\right) + \widehat{\nu} \left(\nabla \left(u_j^{n+1} - u_j^n\right), \nabla v\right) = \langle f_j^{n+1}, v \rangle.$$
(16)

We consider the following approximation of (14):

$$\frac{|R_{j}^{n+1}|^{2} - |R_{j}^{n}|^{2}}{\tau} = -\xi_{j}^{n+1}\nu_{j}\|\nabla\overline{u}_{j}^{n+1}\|^{2} - \widehat{\nu}\frac{\xi_{j}^{n+1}\|\nabla\overline{u}_{j}^{n+1}\|^{2} - \xi_{j}^{n}\|\nabla\overline{u}_{j}^{n}\|^{2}}{2} \\
-\xi_{j}^{n+1}\left\langle\frac{\Theta_{1}\left(u_{j}^{n}\cdot\mathbf{n}\right)u_{j}^{n}\cdot\mathbf{n}}{2}, |\overline{u}_{j}^{n+1}|^{2}\right\rangle_{N} \\
\underline{-\left\langle\widehat{\sigma}_{1}\left(\widehat{u}_{j}^{n+1}, \widehat{p}_{j}^{n+1}\right), g_{j}^{n+1}\right\rangle_{D} + \left(f_{j}^{n+1}, \widehat{u}_{j}^{n+1}\right)}_{:=A_{0}} \\
\underline{-\xi_{j}^{n+1}\left\langle\sigma_{1}\left(\widetilde{u}_{j}^{n+1}, \widehat{p}_{j}^{n+1}\right), g_{j}^{n+1}\right\rangle_{D} + \xi_{j}^{n+1}\left(f_{j}^{n+1}, \widetilde{u}_{j}^{n+1}\right)}_{:=\xi_{j}^{n+1}A_{1}} \\
+\left(1-\xi_{j}^{n+1}\right)|A_{0}| + \left(1-\xi_{j}^{n+1}\right)|A_{1}|, \tag{17}$$

where

$$u_j^{n+1} := \widehat{u}_j^{n+1} + \xi_j^{n+1} \widetilde{u}_j^{n+1}, \overline{u}_j^{n+1} := \widehat{u}_j^{n+1} + \widetilde{u}_j^{n+1}, p_j^{n+1} := \widehat{p}_j^{n+1} + \xi_j^{n+1} \widetilde{p}_j^{n+1},$$

$$R_j(t^{n+1}) \simeq \frac{R_j^{n+1} + R_j^n}{2}.$$
(18)

We emphasize that the additional terms  $(1 - \xi_j^{n+1}) |A_0|$  and  $(1 - \xi_j^{n+1}) |A_1|$  are consistent terms, and are meant to ensure the positivity of the scalar auxiliary variables. The idea was originally put forth in [18], although our implementation is much simpler.

# 3.2. Second order scheme

To discuss the second order scheme, we consider the following perturbation of the momentum equation (1) and the open boundary condition (9):

$$\partial_t u_j + \xi_j u_j \cdot \nabla u_j - \nu_j \Delta u_j - \tau \alpha \Delta \partial_t u_j - \tau^2 \nu_\infty \Delta \partial_{tt} u_j + \nabla p_j = f_j$$
 (19)

and

$$\underbrace{\left(-\nu_{j}\nabla u_{j} - \alpha\tau\nabla\partial_{t}u_{j} - \nu_{\infty}\tau^{2}\nabla\partial_{tt}u_{j} + p_{j}\mathbf{I}\right)\mathbf{n}}_{:=\sigma_{2}(u_{j},p_{j})} = -\xi_{j}\frac{\Theta_{0}\left(u_{j}\cdot\mathbf{n}\right)u_{j}\cdot\mathbf{n}}{2}u_{j} \text{ on } \Gamma_{N}.$$
(20)

To be formally second order accurate, we will pick  $\alpha = h$  in numerical simulations, where h is the mesh diameter.

Upon multiplying (19) by a test function  $v \in H^1(\Omega)$  and integrating by parts, we obtain

$$(\partial_t u_j, v) + \xi_j \sum_{i=1}^2 b_i(u_j, u_j, v) + \nu_j (\nabla u_j, \nabla v) + \tau \alpha (\nabla \partial_t u_j, \nabla v)$$

$$+ \tau^2 \nu_\infty (\nabla \partial_{tt} u_j, \nabla v) - (p_j, \nabla \cdot v) + \langle \sigma_2(u_j, p_j), v \rangle_D = \langle f_j, v \rangle$$
(21)

Then the equation for  $R_i$  can be written as

$$2R_{j}\partial_{t}R_{j} = (\partial_{t}u_{j}, u_{j})$$

$$= (\partial_{t}u_{j}, u_{j}) + \xi_{j} \sum_{i=1}^{2} b_{i} (u_{j}, u_{j}, u_{j}) - \left\langle \frac{g_{j} \cdot \mathbf{n}}{2} g_{j}, g_{j} \right\rangle_{D}$$

$$- \xi_{j} \left\langle \frac{\Theta_{1} (u_{j} \cdot \mathbf{n}) u_{j} \cdot \mathbf{n}}{2}, |u_{j}|^{2} \right\rangle_{N} \text{ (now use (21) with } v = u_{j}) \qquad (22)$$

$$= -\xi_{j} \nu_{j} ||\nabla u_{j}||^{2} - \tau \xi_{j} \alpha \partial_{t} \frac{||\nabla u_{j}||^{2}}{2} - \xi_{j} \left\langle \frac{\Theta_{1} (u_{j} \cdot \mathbf{n}) u_{j} \cdot \mathbf{n}}{2}, |u_{j}|^{2} \right\rangle_{N}$$

$$- \tau^{2} \nu_{\infty} (\nabla \partial_{tt} u_{j}, \nabla u_{j}) - \langle \widehat{\sigma}_{2} (u_{j}, p_{j}), g_{j} \rangle_{D} + \langle f_{j}, u_{j} \rangle,$$

where  $\widehat{\sigma}_2(u_j, p_j) := \sigma_2(u_j, p_j) + \frac{g_j \cdot \mathbf{n}}{2} g_j$ . Unlike the first order case, setting  $f_j = g_j = 0$ , and integrating (22) over time from 0 to t, we do not quite get the unconditional stability. Here, the "hyperbolic" regularization term  $\tau^2 \nu_{\infty} (\nabla \partial_{tt} u_j, \nabla u_j)$  spoils the game. Nonetheless, we can still obtain a second-order discrete scheme that is unconditionally stable, as will be derived below.

To this end, let  $u^{*,n+1} := 2u^n - u^{n-1}$  and

$$D_t u^{n+1} = \frac{3u^{n+1} - 4u^n + u^{n-1}}{2\tau}, \quad D_{tt} u^{n+1} = \frac{u^{n+1} - 2u^n + u^{n-1}}{\tau^2}.$$

The Navier-Stokes part of the discrete system is obtained from (19) by restricting the test functions to  $X_D$ :

$$(D_t u_j^{n+1}, v) + \xi_j \sum_{i=1}^2 b_i(u_j^{*,n+1}, u_j^{*,n+1}, v) + \nu_j \left(\nabla u_j^{*,n+1}, \nabla v\right)$$
(23)

$$+\alpha\tau\left(\nabla D_{t}u_{j}^{n+1},\nabla v\right)+\tau^{2}\nu_{\infty}\left(\nabla D_{tt}u_{j}^{n+1},\nabla v\right)-\left(p_{j}^{n+1},\nabla \cdot v\right)=\left\langle f_{j}^{n+1},v\right\rangle$$

As in [18], we approximate  $\xi_j$  at the time level  $n + \frac{3}{2}$  via a second order extrapolation. To this end, we let

$$R_j^{n+3/2} := \frac{3}{2}R_j^{n+1} - \frac{1}{2}R_j^n$$
,

$$\begin{split} \overline{u}_{j}^{n+3/2} &:= \frac{3}{2} \overline{u}_{j}^{n+1} - \frac{1}{2} u_{j}^{n} \,, \\ 2R_{j}(t^{n+1}) &\simeq \frac{3}{2} R_{j}^{n+1} + R_{j}^{n} - \frac{1}{2} R_{j}^{n-1} = R_{j}^{n+3/2} - R_{j}^{n+1/2} \,, \\ E\left[\overline{u}_{j}^{n+3/2}\right] &= \frac{\|\overline{u}_{j}^{n+3/2}\|^{2}}{2} + C_{0} \,, \\ \xi(t) &\simeq \xi_{j}^{n+3/2} &= \frac{R_{j}^{n+3/2}}{E\left[\overline{u}_{j}^{n+3/2}\right]} \,, \\ \overline{E}_{j}^{n+3/2} &:= \frac{\|\nabla \overline{u}_{j}^{n+1}\|^{2} + \|\nabla (2\overline{u}_{j}^{n+1} - u_{j}^{n})\|^{2}}{4} \,, \\ D_{j}^{n+1} &:= \frac{\|\nabla (\overline{u}_{j}^{n+1} - 2u_{j}^{n} + u_{j}^{n-1})\|^{2}}{4} \,. \end{split}$$

Using the identity

$$\left(\frac{3}{2}R_j^{n+1} + R_j^n - \frac{1}{2}R_j^{n-1}\right)\left(\frac{3}{2}R_j^{n+1} - 2R_j^n + \frac{1}{2}R_j^{n-1}\right) = |R_j^{n+3/2}|^2 - |R_j^{n+1/2}|^2,$$

and by approximating the term

$$\partial_t \frac{\|\nabla u_j\|^2}{2} = (\partial_t \nabla u_j, \nabla u_j)$$

via the BDF2 discretization, we consider the following approximation of (22):

$$\frac{\left|R_{j}^{n+3/2}\right|^{2} - \left|R_{j}^{n+1/2}\right|^{2}}{\tau} = -\xi_{j}^{n+3/2}\nu_{j}\|\nabla\overline{u}_{j}^{n+1}\|^{2} - \alpha\xi_{j}^{n+3/2}D_{j}^{n+1} 
- \alpha\left(\xi_{j}^{n+3/2}\overline{E}_{j}^{n+3/2} - \xi_{j}^{n+1/2}\overline{E}_{j}^{n+1/2}\right) 
- \xi_{j}^{n+3/2}\left\langle\frac{\Theta_{1}\left(u_{j}^{*,n+1}\cdot\mathbf{n}\right)u_{j}^{*,n+1}\cdot\mathbf{n}}{2}, |\overline{u}_{j}^{n+1}|^{2}\right\rangle_{N} (24) 
\underline{-\left\langle\widehat{\sigma}\left(\widehat{u}_{j}^{n+1},\widehat{p}_{j}^{n+1}\right),g_{j}\right\rangle_{D} + \left\langle f_{j}^{n+1},\widehat{u}_{j}^{n+1}\right\rangle} 
\vdots = A_{0} 
\underline{-\xi_{j}^{n+3/2}\left\langle\widehat{\sigma}\left(\widetilde{u}_{j}^{n+1},\widehat{p}_{j}^{n+1}\right),g_{j}\right\rangle_{D} + \xi_{j}^{n+3/2}\left\langle f_{j}^{n+1},\widetilde{u}_{j}^{n+1}\right\rangle} 
\vdots = \xi_{j}^{n+3/2}A_{1} 
+ \left(1 - \xi_{j}^{n+3/2}\right)|A_{0}| + \left(1 - \xi_{j}^{n+3/2}\right)|A_{1}|.$$

Notice that the contribution of the  $\tau^2$  term in (19) to the energy equation is simply omitted in (24), which does not introduce any inconsistency into the

system. Moreover, in the definitions of  $A_0$  and  $A_1$ , we have approximated  $\hat{\sigma}_2$  and  $\sigma_2$  with  $\hat{\sigma}$  and  $\sigma$ , respectively.

Remark 3.1. The presence of the second  $\alpha$ -stabilizing term in equations (17) and (24) might seem redundant. Note that for the ensemble equation with  $\nu_j = \nu_\infty$ , the alpha-regularization term is needed for the SAV scheme to converge. And, due to the coupled nature of system, the entire ensemble system also requires that term. Our numerical tests also confirmed these arguments.

## 3.3. Stability

**Theorem 3.2.** Assuming  $f_j = g_j = 0$ , both schemes (16)-(17), and (23)-(24) are unconditionally stable.

**Proof 3.3.** Under our assumptions, the "energy" equation for the first order scheme becomes

$$\frac{|R_{j}^{n+1}|^{2} - |R_{j}^{n}|^{2}}{\tau} = -\xi_{j}^{n+1}\nu_{j}\|\nabla\overline{u}_{j}^{n+1}\|^{2} - \widehat{\nu}\frac{\xi_{j}^{n+1}\|\nabla\overline{u}_{j}^{n+1}\|^{2} - \xi_{j}^{n}\|\nabla\overline{u}_{j}^{n}\|^{2}}{2} - \xi_{j}^{n+1}\left\langle\frac{\Theta_{1}\left(u_{j}^{n}\cdot\mathbf{n}\right)u_{j}^{n}\cdot\mathbf{n}}{2}, |\overline{u}_{j}^{n+1}|^{2}\right\rangle_{N}.$$
(25)

Multiplying both sides by  $\tau$  and summing over the timesteps from n=0 to N-1 gives

$$|R_{j}^{N}|^{2} + \tau \xi_{j}^{N} \widehat{\nu} \frac{\|\nabla \overline{u}_{j}^{N}\|^{2}}{2} = |R_{j}^{0}|^{2} + \tau \xi_{j}^{0} \widehat{\nu} \frac{\|\nabla \overline{u}_{j}^{0}\|^{2}}{2}$$

$$-\tau \sum_{n=0}^{N-1} \xi_{j}^{n+1} \left(\nu_{j} \|\nabla \overline{u}_{j}^{n+1}\|^{2} + \left\langle \frac{\Theta_{1} \left(u_{j}^{n} \cdot \mathbf{n}\right) u_{j}^{n} \cdot \mathbf{n}}{2}, |\overline{u}_{j}^{n+1}|^{2} \right\rangle_{N} \right)$$

$$\Longrightarrow |R_{j}^{N}|^{2} + \tau \xi_{j}^{N} \widehat{\nu} \frac{\|\nabla \overline{u}_{j}^{N}\|^{2}}{2} \leq |R_{j}^{0}|^{2} + \tau \widehat{\nu} \frac{\|\nabla \overline{u}_{j}^{0}\|^{2}}{2}.$$
(26)

The stability of the second order scheme is established in a similar way. The "energy" equation of the scheme simplifies down to

$$\frac{\left|R_{j}^{n+3/2}\right|^{2} - \left|R_{j}^{n+1/2}\right|^{2}}{\tau} = -\xi_{j}^{n+3/2} \left(\nu_{j} \|\nabla \overline{u}_{j}^{n+1}\|^{2} + D_{j}^{n+1}\right) -\alpha \left(\xi_{j}^{n+3/2} \overline{E}_{j}^{n+3/2} - \xi_{j}^{n+1/2} \overline{E}_{j}^{n+1/2}\right) \tag{27}$$

$$-\xi_j^{n+3/2} \left\langle \frac{\Theta_1 \left( u_j^{*,n+1} \cdot \mathbf{n} \right) u_j^{*,n+1} \cdot \mathbf{n}}{2}, |\overline{u}_j^{n+1}|^2 \right\rangle_N.$$

Multiplying both sides of (27) by  $\tau$  and summing over the timesteps from n=0 to N-1 gives

$$\left| R_{j}^{N+3/2} \right|^{2} + \tau \xi_{j}^{N+3/2} \alpha \overline{E}_{j}^{N+3/2} = \left| R_{j}^{1/2} \right|^{2} + \tau \xi_{j}^{1/2} \alpha \frac{\|\nabla \overline{u}_{j}^{1/2}\|^{2}}{2} \qquad (28)$$

$$-\tau \sum_{n=0}^{N-1} \xi_{j}^{n+3/2} \left( \nu_{j} \|\nabla \overline{u}_{j}^{n+1}\|^{2} + D_{j}^{n+1} + \left\langle \frac{\Theta_{1} \left( u_{j}^{*,n+1} \cdot \mathbf{n} \right) u_{j}^{*,n+1} \cdot \mathbf{n}}{2}, |\overline{u}_{j}^{n+1}|^{2} \right\rangle_{N} \right).$$

$$\Rightarrow \left| R_{j}^{N+3/2} \right|^{2} + \tau \xi_{j}^{N+3/2} \alpha \frac{\|\nabla \overline{u}_{j}^{N+3/2}\|^{2}}{2} \leq \left| R_{j}^{1/2} \right|^{2} + \tau \xi_{j}^{1/2} \alpha \frac{\|\nabla \overline{u}_{j}^{1/2}\|^{2}}{2}.$$

## 20 4. Solution algorithm

Herein we describe an efficient procedure for solving the proposed schemes. For the sake of brevity, we only concentrate on the second order scheme (23)-(24).

Using the decomposition (18), we solve for  $(\widehat{u}_i^{n+1}, \widehat{p}_i^{n+1})$ :

$$\left(\frac{3\widehat{u}_{j}^{n+1} - 4u_{j}^{n} + u_{j}^{n-1}}{2\tau}, v\right) + \nu_{\infty} \left(\nabla \left(\widehat{u}_{j}^{n+1} - 2u_{j}^{n} + u_{j}^{n-1}\right), \nabla v\right) 
+ \frac{\alpha}{2} \left(\nabla \left(3\widehat{u}_{j}^{n+1} - 4u_{j}^{n} + u_{j}^{n-1}\right), \nabla v\right) + \nu_{j} \left(\nabla u_{j}^{*,n+1}, \nabla v\right) 
- \left(\widehat{p}_{j}^{n+1}, \nabla \cdot v\right) = \left(f_{j}^{n+1}, v\right),$$

$$\left(q, \nabla \cdot \widehat{u}_{j}^{n+1}\right) = 0,$$

$$\widehat{u}_{j}^{n+1} = g_{j}^{n+1} \text{ on } \Gamma_{D},$$
(29)

and for  $(\widetilde{u}^{n+1}, \widetilde{p}^{n+1})$ :

$$\left(\frac{3\widetilde{u}_{j}^{n+1}}{2\tau}, v\right) + \sum_{i=1}^{2} b_{i}(u_{j}^{*,n+1}, u_{j}^{*,n+1}, v) + \frac{3\alpha}{2} \left(\nabla \widetilde{u}_{j}^{n+1}, \nabla v\right) 
+ \nu_{\infty} \left(\nabla \widetilde{u}_{j}^{n+1}, \nabla v\right) - \left(\widetilde{p}_{j}^{n+1}, \nabla \cdot v\right) = 0, 
\left(q, \nabla \cdot \widetilde{u}_{j}^{n+1}\right) = 0,$$

$$\widetilde{u}_{j}^{n+1} = 0 \text{ on } \Gamma_{D}.$$
(30)

We then obtain 
$$\overline{u}_{j}^{n+1}$$
 and  $\overline{u}_{j}^{n+3/2}$ ,  $E\left[\overline{u}_{j}^{n+3/2}\right] = \frac{\left\|\overline{u}_{j}^{n+3/2}\right\|^{2}}{2} + C_{0}$  and using  $\xi_{j}^{n+3/2} = \frac{|R_{j}^{n+3/2}|^{2}}{E\left[\overline{u}_{j}^{n+3/2}\right]}$ , algebraically compute  $|R_{j}^{n+3/2}|^{2}$  from (24):

$$S_{0} := \nu_{j} \|\nabla \overline{u}_{j}^{n+1}\|^{2} + \alpha \left(\overline{E}_{j}^{n+3/2} + D_{j}^{n+1}\right) + |A_{0}| + |A_{1}| - A_{1}$$

$$+ \left\langle \frac{\Theta_{1} \left(u_{j}^{*,n+1} \cdot \mathbf{n}\right) u_{j}^{*,n+1} \cdot \mathbf{n}}{2}, |\overline{u}_{j}^{n+1}|^{2} \right\rangle_{N},$$

$$S_{1} := \alpha \xi_{j}^{n+1/2} \overline{E}_{j}^{n+1/2} + |A_{0}| + A_{0} + |A_{1}|,$$

$$\xi_{j}^{n+3/2} = \frac{\left|R_{j}^{n+1/2}\right|^{2} + \tau S_{1}}{E\left[\overline{u}_{j}^{n+3/2}\right] + \tau S_{0}}.$$
(31)

# 5. Numerical experiments

The simulations are performed using the FreeFem++ [30] package, with the  $(P_2, P_1)$  used to approximate the velocity and pressure spaces, respectively. We only tested the second order scheme and all the linear systems are solved using direct solvers.

# 5.1. Flow around a cylinder

Our first test is on a two dimensional channel flow around a cylinder, a well-known benchmark problem taken from Shäfer and Turek [31]. The domain for the problem is a  $2.2 \times 0.41$  rectangular channel with a cylinder of radius 0.05 centered at (0.2, 0.2) (taking the bottom left corner of the rectangle as the origin). The cylinder, top and bottom of the channel are prescribed no slip boundary conditions, and the time dependent inflow profile is

$$u_1(0, y, t) = u_1(2.2, y, t) = \frac{6}{0.41^2} \sin(\pi t/8) y (0.41 - y),$$
  
$$u_2(0, y, t) = u_2(2.2, y, t) = 0.$$

The open boundary conditions (9) are used for the outflow. In order to test the robustness of our algorithm with respect to the location of the open boundary, we also simulated the problem on a truncated domain, where the right

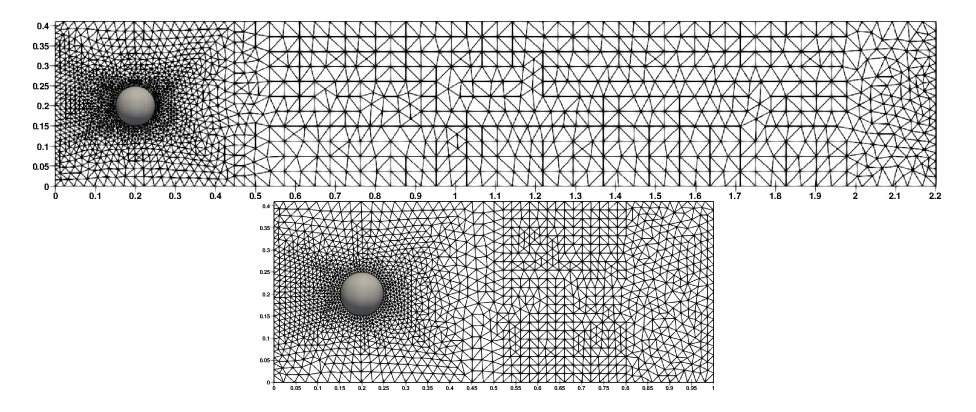


Figure 1: The finite element meshes used in flow around a cylinder experiment.

x-boundary is located at x=1. The reference results for this in the case of the full domain problem with  $\nu=\frac{1}{1000}$  are given in [32] for the Dirichlet outflow.

135

Here we chose three ensemble members. The viscosities are  $\nu_1 = \frac{1}{1000}$ ,  $\nu_2 = \frac{1}{900}$ ,  $\nu_3 = \frac{1}{800}$  and  $\alpha = h$ . We compare the results of the  $\nu_1$  case with the reference values. The finite element meshes used in the simulations are shown in Fig. 1 with mesh size h = 0.0216741. The timestep is  $\Delta t = 0.004$ .

We compute values for the maximal drag  $c_{d,max}$  and lift  $c_{l,max}$  coefficients on the cylinder boundary, and the pressure difference  $\Delta p(t)$  between the front and back of the cylinder at the final time T=8. The time evolutions of the these quantities are given in Fig. 2, and in both cases we get almost identical results. A slight difference is observed in the evolution of  $c_l$  towards the end of the simulation, which can be attributed to the well-known sensitivity of this quantity to perturbations. The maximum lift and drag coefficients and pressure drop for the simulations are given in Table 1. In general, we observe results that are close to the reference values.

The velocity field plots at times t=6,8 are presented in Fig. 3 for both simulation domains, which show the expected vortex street and close agreement between the results of both domains.

As a qualitative reference, we can compare our results with those of [33] where the do-nothing outflow boundary condition was used. It would be inap-

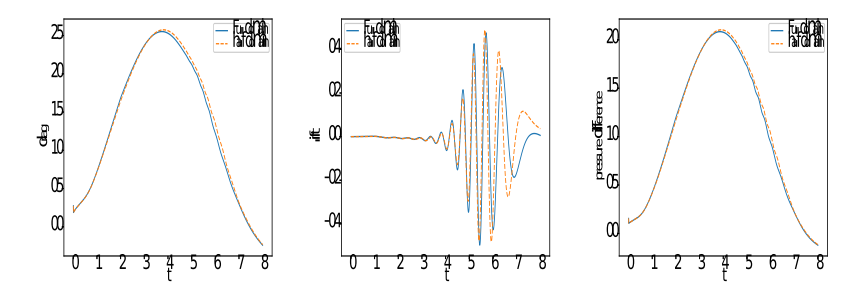


Figure 2: From left to right: the drag and lift coefficients  $c_d$ ,  $c_l$  and pressure difference between front and back of the cylinder  $\Delta p$  for flow past a cylinder with full domain and half domain

 $t(c_{l,max})$ domain size  $\Delta p$  $t(c_{d,max})$  $c_{d,max}$  $c_{l,max}$ 2.94934 3.944 0.4766015.708 full domain -0.103358half domain 2.949280.489891-0.1045993.936 5.66Dirichlet) [32] 2.950923.936255.6925 -0.11160.47788(No-traction) [33] 2.9513 4.01120.478875.6928 -0.026382

Table 1: Drag, Lift and pressure drop values

propriate to use the solution of [32] for comparison, as the prescribed Dirichlet type parabolic outflow profile is less physical. For instance, [32] predicts that at t=8 the last eddy will remain on the left hand side of x=2.2 completely, while following the previous alternating pattern from upstream, it is unrealistic that both eddies near the top and bottom walls will vanish at the same position at x=2.2. In both of our simulations, the last eddy is cut through by the outflow boundary, which agrees with the results in [33].

# 5.2. Channel flow with a contraction and two outlets

Our next experiment is for a complex 2D flow through a channel with a contraction and two outlets, one on the top of the channel and the other at the end of the channel. The finite element mesh with 16,672 DOF used in the test is shown in Fig. 4. Even though this flow occurs at Re = 1000, we found it to be a very challenging test problem for SAV schemes.

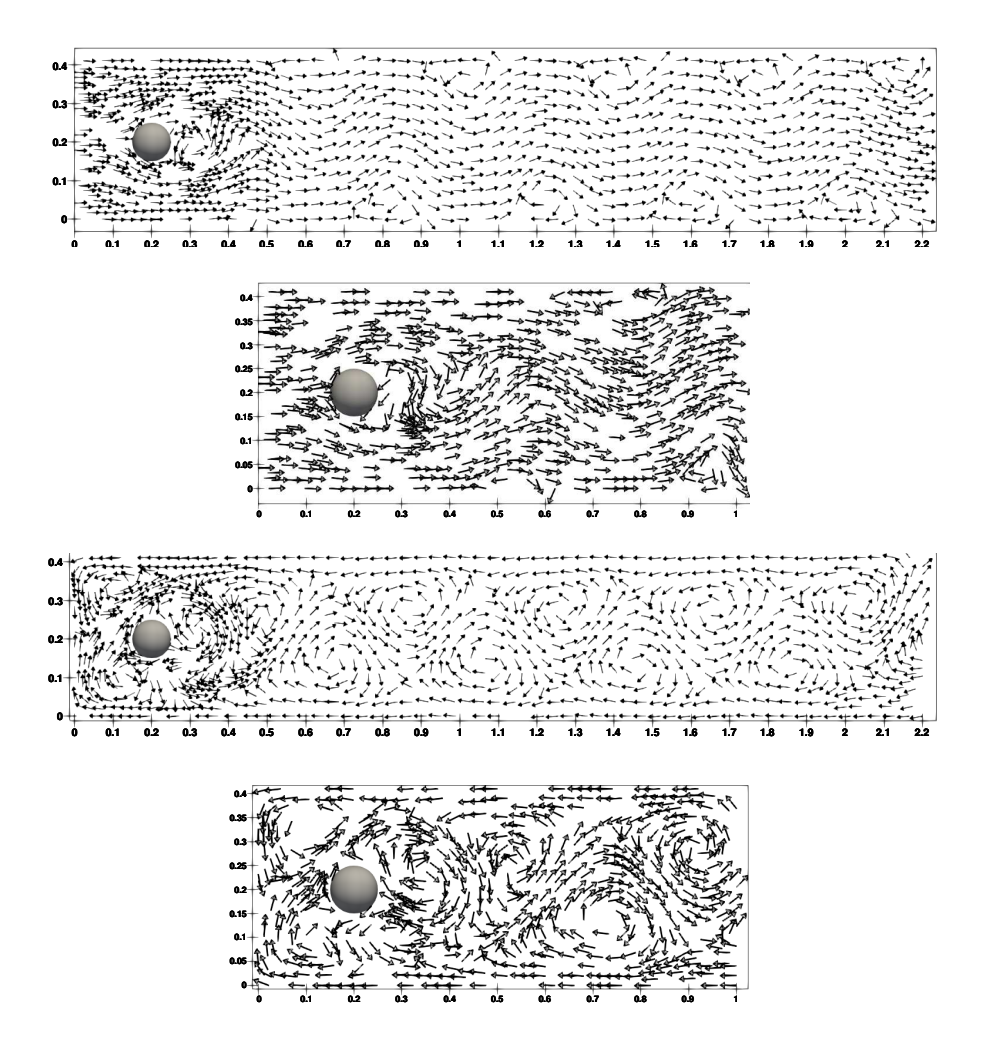


Figure 3: Speed contours at t=6 (top) and at t=8 (bottom)

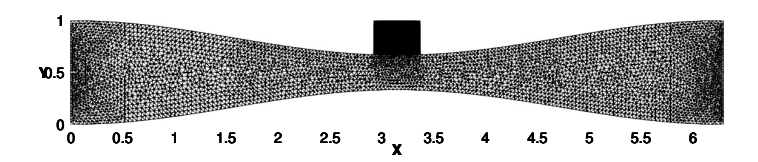


Figure 4: The finite element mesh used in Channel flow with a contraction and two outlets.

Here we again ran the algorithm with three ensemble members on the time interval (0,4), with  $\nu_1=0.001$ ,  $\nu_2=0.003$  and  $\nu_3=0.005$ . The velocity boundary conditions are:

$$g_1 = (4y(1-y), 0)^T, g_2 = (1+\varepsilon)(4y(1-y), 0)^T, g_3 = (1-\varepsilon)(4y(1-y), 0)^T$$

at the inlet, open boundary condition at the top and right boundaries and noslip on the remaining walls. Initial conditions  $u_{1,h}^0, u_{2,h}^0, u_{3,h}^0$  are obtained by solving the Stokes equations in the same domain with perturbed body forces

$$f_1 = \varepsilon(0,0)^T$$
,  $f_2 = \varepsilon(\cos(\pi xy + t), \sin(\pi(x+y) + t))^T$  and 
$$f_3 = \varepsilon(\sin(\pi(x+y) + t), \cos(\pi xy + t))^T$$

with  $\varepsilon = 10^{-2}$ .

We tested the result with two different values of  $\alpha$ :  $\alpha = h$  and  $\alpha = 0$ . The speed contours for both cases are given in Fig. 6 and Fig. 7, respectively. While the ensemble scheme with the  $\alpha = h$  gives results that qualitatively match the references plots of [34], the simulations with  $\alpha = 0$  did not produce physically accurate solutions. Concretely, at t = 4 the jet has not yet reached the outflow boundary and also seems to assume an incorrect profile. Similar lagging behavior is observed at t = 1.

The explanation for this difference between two cases can be understood by looking at the time evolution of  $\xi$ , given in Fig. 5. As it can be observed, in the  $\alpha = h$  case, all  $\xi_i$ 's are very close to 1. On the other hand,  $\alpha = 0$  simulations produce the values of  $\xi_i$ 's that are as low as 0.1. Thus, the  $\alpha = 0$  case predicts advective term that is not as large as it should be.

# 5.3. Jet Impinging on a Wall

As a last test problem, a 2D jet impinging on a solid wall is tested with our method. Due to the open boundaries and the physical instability of the jet, the open boundary condition is critical to the successful simulation of this flow. This problem has been studied with different Reynolds numbers in [35]. Here we will test the case of Re = 300 where the flows reach the steady state.

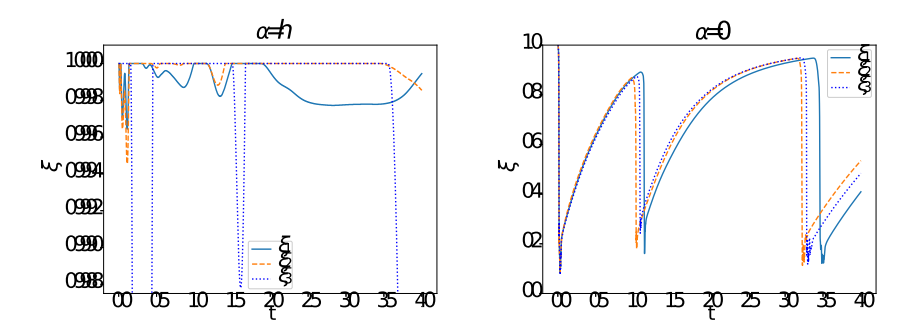


Figure 5:  $\xi_i$  for three ensemble members with  $\alpha=h$  (left) and  $\alpha=0$  (right)

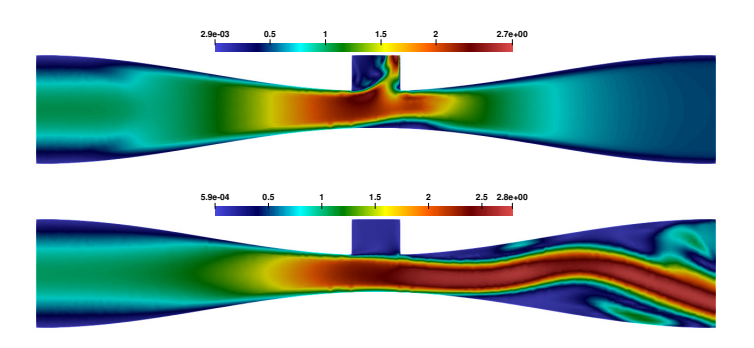


Figure 6: Plots of speed contour for  $\nu_1$  at t=1 (top) and t=4 (bottom) with  $\alpha=h$  .

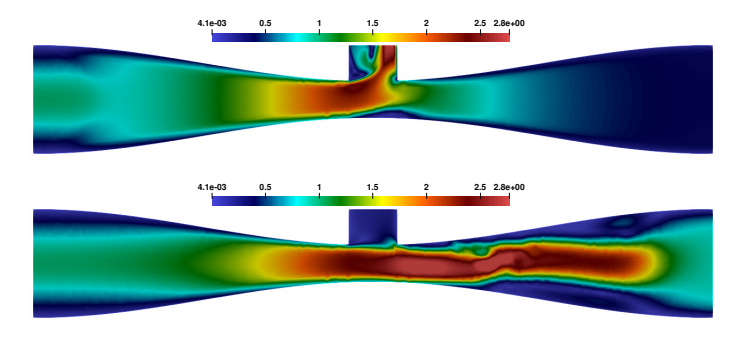


Figure 7: Plots of speed contour for  $\nu_1$  at t=1 (top) and t=4 (bottom) with  $\alpha=0$ .

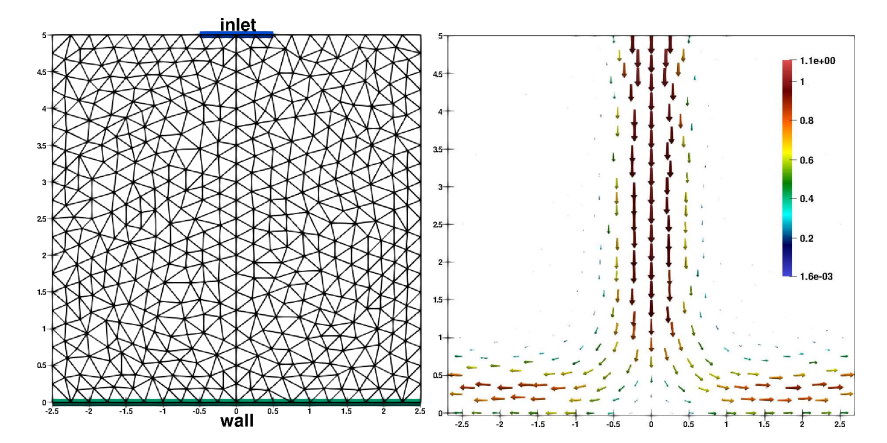


Figure 8: The boundary conditions and the mesh (left); velocity field (right).

The same simulation set-up is used as in [35]. A fluid jet with diameter d is impinging on a 2D wall with the dimension of  $-\frac{5}{2}d \le x \le \frac{5}{2}d$  and  $0 \le y \le 5d$ . The bottom of the domain is a solid wall while the jet is coming in from the top center of the domain, hence the inlet is  $-R_0 \le R_0$  and y = 5d, where  $R_0$  is the radius of the jet  $(R_0 = \frac{d}{2})$ . The jet velocity profile at the inlet is given as:

$$\begin{cases} u = 0, \\ v = -U_0 \left[ \tanh \frac{1 - \frac{x}{R_0}}{\sqrt{2} \frac{\epsilon}{d}} (H(x, 0) - H(x, R_0) + \tanh \frac{1 + \frac{x}{R_0}}{\sqrt{2} \frac{\epsilon}{d}} (H(x, -R_0) - H(x, 0)) \right], \end{cases}$$

where  $U_0$  is the velocity scale  $(U_0 = 1)$ ,  $\epsilon = \frac{1}{40}d$ , and H(x,a) is the unit step function, which is the unit value when  $x \geq a$  and zero otherwise. Herein we considered three ensemble members with viscosities  $\nu_1 = \frac{1}{300}$ ,  $\nu_2 = \frac{1}{250}$ ,  $\nu_3 = \frac{1}{350}$  and  $\alpha = h$ . The boundaries on the left, right and the top excluding the inlet are all open boundaries where our open boundary condition (9) will be applied. Noslip boundary condition is used for the bottom wall. The domain, its boundary description and the mesh with h = 0.37544 are shown in Figure 8. The time step is  $\Delta t = 0.004$ .

For the Reynolds number we are running with (Re = 300), the flow reaches a steady state. The simulation is ran until it  $\|\frac{du}{dt}\| < 10^{-6}$ . The vertical incoming jet splits into two horizontal streams as it hits the bottom wall and proceed in opposite directions parallel to the bottom wall until they exit the domain. In

Table 2: Vertical force on the bottom wall

method	$f_y$
OBC from our algorithm	-0.9875
OBC-B and OBC-C from [35]	-0.994
Traction-fee OBC from [35]	-1.026

regions of the domain outside the jet stream the velocity appears to be negligibly small. With our open boundary condition (9), the flow exits the domain without any reflection or any instability, see Fig. 8. Qualitatively, an excellent match can be observed between our results and the reference velocity field plot in [35].

We also computed the y-component of the force on the bottom wall and compared with the results from [35], reported in the Table 2. Even with the relatively coarse mesh, good quantitative agreements can be observed.

#### 6. Conclusions

200

We have presented two robust ensemble algorithms for computing the Navier-Stokes flow ensembles. Both algorithms (16)-(17), and (23)-(24) require a single matrix assembly for all realizations and all time steps, and lead to linear systems that have one common constant coefficient matrix with multiple right hand sides, which can be solved at significantly reduced computational cost compared with traditional, nonensemble algorithms for flow ensemble simulations. We proved both algorithms are unconditionally stable without any timestep conditions or assumption on the variance of the viscosities. We also presented three benchmark flow problems with open boundaries, which showed our algorithms are robust and effective in preventing backflow instabilities producing physical and accurate flow statistics.

#### References

[1] P. Sagaut, T. H. Lê, Some investigations on the sensitivity of Large Eddy Simulation, in: J.-P. Chollet, P. R. Voke, L. Kleiser (Eds.), Direct and

Large-Eddy Simulation II, Springer Netherlands, Dordrecht, 1997, pp. 81–92.

215

220

230

235

240

- [2] M. R. D. Carati, A. Wray, Statistical ensemble of large-eddy simulations,J. Fluid Mech. 455 (2002) 195–212.
- [3] V. S. C. Hasse, B. Durst, Numerical investigation of cyclic variations in gasoline engines using a hybrid uransles modeling approach, Comput. Fluids 39 (2010) 25–48.
- [4] Z. Toth, E. Kalnay, Ensemble forecasting at ncep and the breeding method, Monthly Weather Review 125 (12) (1997) 3297-3319. arXiv:https://doi.org/10.1175/1520-0493(1997)125<3297:EFANAT>2.0.CO;2, doi: 10.1175/1520-0493(1997)125<3297:EFANAT>2.0.CO;2.
- URL https://doi.org/10.1175/1520-0493(1997)125<3297:EFANAT>2.
  0.CO;2
  - [5] M. Leutbecher, T. Palmer, Ensemble forecasting, Journal of Computational Physics 227 (7) (2008) 3515–3539, predicting weather, climate and extreme events. doi:https://doi.org/10.1016/j.jcp.2007.02.014.
  - URL https://www.sciencedirect.com/science/article/pii/ S0021999107000812
  - [6] U. M. Ascher, S. J. Ruuth, R. J. Spiteri, Implicit-explicit runge-kutta methods for time-dependent partial differential equations, Applied Numerical Mathematics 25 (2) (1997) 151–167, special Issue on Time Integration. doi:https://doi.org/10.1016/S0168-9274(97)00056-1.
    - URL https://www.sciencedirect.com/science/article/pii/S0168927497000561
  - [7] K. Jbilou, Smoothing iterative block methods for linear systems with multiple right-hand sides, Journal of Computational and Applied Mathematics 107 (1) (1999) 97 109. doi:http://dx.doi.org/10.1016/S0377-0427(99)00083-7.

- URL http://www.sciencedirect.com/science/article/pii/S0377042799000837
- [8] M. Heyouni, A. Essai, Matrix krylov subspace methods for linear systems
   with multiple right-hand sides, Numerical Algorithms 40 (2) (2005) 137–156. doi:10.1007/s11075-005-1526-2.
   URL https://doi.org/10.1007/s11075-005-1526-2
  - [9] N. Jiang, W. Layton, An algorithm for fast calculation of flow ensembles, International Journal for Uncertainty Quantification 4 (4) (2014) 273–301.
- [10] N. Jiang, W. Layton, Numerical analysis of two ensemble eddy viscosity numerical regularizations of fluid motion, Numerical Methods for Partial Differential Equations 31 (3) (2015) 630-651. doi:10.1002/num.21908.
  URL http://dx.doi.org/10.1002/num.21908
- [11] N. Jiang, A higher order ensemble simulation algorithm for fluid flows,
   Journal of Scientific Computing 64 (1) (2015) 264–288. doi:10.1007/s10915-014-9932-z.
   URL https://doi.org/10.1007/s10915-014-9932-z
  - [12] M. N. A. Takhirov, J. Waters, Time relaxation algorithm for flow ensembles, Numerical Methods for Partial Differential Equations 32 (3) (2016) 757-777. doi:10.1002/num.22024.
    URL http://dx.doi.org/10.1002/num.22024

260

[13] M. Gunzburger, N. Jiang, Z. Wang, An efficient algorithm for simulating ensembles of parameterized flow problems, IMA Journal of Numerical Analysis (2018) dry029arXiv:/oup/backfile/content\_public/journal/imajna/pap/10.1093\_imanum\_dry029/2/dry029.pdf, doi:10.1093/imanum/dry029.

URL http://dx.doi.org/10.1093/imanum/dry029

[14] A. Takhirov, J. Waters, Ensemble algorithm for parametrized flow problems with energy stable open boundary conditions, Computational Methods in Applied Mathematics 20 (3) (2020) 531-554. doi:doi:10.1515/cmam-2018-0203.

URL https://doi.org/10.1515/cmam-2018-0203

275

S002199911730774X

[15] M. Gunzburger, N. Jiang, Z. Wang, A second-order time-stepping scheme for simulating ensembles of parameterized flow problems, Computational Methods in Applied Mathematics 19 (2019)) 681–701. doi:10.1515/cmam-2017-0051.

URL https://www.degruyter.com/document/doi/10.1515/cmam-2017-0051/html

- [16] J. Shen, J. Xu, J. Yang, The scalar auxiliary variable (SAV) approach for gradient flows, Journal of Computational Physics 353 (2018) 407-416. doi:https://doi.org/10.1016/j.jcp.2017.10.021. URL https://www.sciencedirect.com/science/article/pii/
- [17] L. Lin, Z. Yang, S. Dong, Numerical approximation of incompressible navier-stokes equations based on an auxiliary energy variable, Journal of Computational Physics 388 (2019) 1-22. doi:https://doi.org/10.1016/j.jcp.2019.03.012.

  URL https://www.sciencedirect.com/science/article/pii/S0021999119301950
- [18] L. Lin, X. Liu, S. Dong, A gpav-based unconditionally energy-stable scheme for incompressible flows with outflow/open boundaries, Computer Methods in Applied Mechanics and Engineering 365 (2020) 112969. doi:https://doi.org/10.1016/j.cma.2020.112969.
  URL https://www.sciencedirect.com/science/article/pii/S0045782520301523
  - [19] X. Li, J. Shen, Error analysis of the sav-mac scheme for the navier–stokes equations, SIAM Journal on Numerical Analysis 58 (5) (2020) 2465–2491. arXiv:https://doi.org/10.1137/19M1288267, doi:10.1137/

#### 19M1288267.

300

320

- URL https://doi.org/10.1137/19M1288267
- [20] J. S. Xiaoli Li, Z. Liu, New sav-pressure correction methods for the navier-stokes equations: stability and error analysis, Mathematics of Computationdoi:https://doi.org/10.1090/mcom/3651.
  URL https://www.ams.org/journals/mcom/0000-000-00/
- 05 S0025-5718-2021-03651-0
  - [21] N. Jiang, H. Yang, Stabilized scalar auxiliary variable ensemble algorithms for parameterized flow problems, SIAM Journal on Scientific Computing 43 (4) (2021) A2869-A2896. arXiv:https://doi.org/10.1137/20M1364679, doi:10.1137/20M1364679.
- URL https://doi.org/10.1137/20M1364679
  - [22] Y. Cao, E. Lunasin, E. Titi, Global well-posedness of three-dimensional viscous and inviscid simplified Bardina turbulence models, Commun. Math. Sci. 4 (4) (2006) 823–848.
- [23] A. Takhirov, Voigt regularization for the explicit time stepping of the Hall
   effect term, Geophys. Astro. Fluid. 110 (5) (2016) 409–431.
  - [24] R. L. Sani, P. M. Gresho, Résumé and remarks on the open boundary condition minisymposium, International Journal for Numerical Methods in Fluids 18 (10) (1994) 983-1008. arXiv:https://onlinelibrary.wiley.com/doi/pdf/10.1002/fld.1650181006,
  - doi:10.1002/fld.1650181006.
    - URL https://onlinelibrary.wiley.com/doi/abs/10.1002/fld.
      1650181006
- [25] J. G. Heywood, R. Rannacher, S. Turek, Artificial boundaries and flux and pressure conditions for the incompressible Navier-Stokes equations, Int. J.
   Numer. Meth. Fluids 22 (5) (1996) 325–352.

[26] C. Bertoglio, A. Caiazzo, Y. Bazilevs, M. Braack, M. Esmaily, V. Gravemeier, A. L. Marsden, O. Pironneau, I. E. Vignon-Clementel, W. A. Wall, Benchmark problems for numerical treatment of backflow at open boundaries, International Journal for Numerical Methods in Biomedical Engineering 34 (2) (2018) e2918. arXiv:https://onlinelibrary.wiley.com/doi/pdf/10.1002/cnm.2918, doi:10.1002/cnm.2918.
URL https://onlinelibrary.wiley.com/doi/abs/10.1002/cnm.2918

330

335

340

- [27] S. Dong, J. Shen, A pressure correction scheme for generalized form of energy-stable open boundary conditions for incompressible flows, J. Comput. Phys. 291 (2015) 254 – 278.
- [28] S. Dong, A convective-like energy-stable open boundary condition for simulations of incompressible flows, Journal of Computational Physics 302 (2015) 300 - 328. doi:https://doi.org/10.1016/j.jcp.2015.09.017. URL http://www.sciencedirect.com/science/article/pii/ S0021999115006105
- [29] V. John, Finite Element Methods for Incompressible Flow Problems, 1st Edition, Springer International Publishing, 2016.
- [30] F. Hecht, New development in FreeFem++, J. Numer. Math. 20 (3-4) (2012) 251–265.
- [31] M. Schäfer, S. Turek, The benchmark problem 'flow around a cylinder' flow simulation with high performance computers II, in E.H. Hirschel (Ed.), Notes on Numerical Fluid Mechanics 52, Braunschweig, Vieweg (1996) 547–566.
- [32] V. John, Reference values for drag and lift of a two dimensional timedependent flow around a cylinder, Int. J. Numer. Meth. Fluids 44 (2004) 777–788.
  - [33] J. Liu, Open and traction boundary conditions for the incompressible Navier-Stokes equations, Journal of Computational Physics 228 (19) (2009)

7250 - 7267. doi:https://doi.org/10.1016/j.jcp.2009.06.021.

URL http://www.sciencedirect.com/science/article/pii/
S0021999109003453

[34] A. Takhirov, A. Lozovskiy, Computationally efficient modular nonlinear filter stabilization for high reynolds number flows, Advances in Computational Mathematics 44 (1) (2018) 295–325. doi:10.1007/s10444-017-9544-x.

URL https://doi.org/10.1007/s10444-017-9544-x

355

[35] N. Ni, Z. Yang, S. Dong, Energy-stable boundary conditions based on a quadratic form: Applications to outflow/open-boundary problems in incompressible flows, J. Comput. Phys. 391 (2019) 179–215.